

DTU Compute

Department of Applied Mathematics and Computer Science

**Dynamics of adaptive neuronal networks
A trip to topology and back**

Author

Simon Aertssen
s181603

Supervisor

Erik Martens
Poul Hjorth

February 1st 2020

Contents

Abstract	III
Acknowledgements	III
1 Nomenclature	IV
2 Introduction	5
3 Network Topologies	6
3.1 Representations and properties	6
3.2 Fixed-degree networks	6
3.3 Random / Erdős-Rényi networks	6
3.4 Scale-free networks	7
4 The Theta Neuron Model	8
4.1 Modelling neuronal behaviour	8
4.2 Canonical neuron models	8
4.3 Theta Neuron model description	8
4.4 Solutions for static currents	10
4.5 Frequency response	10
4.6 Phase response	11
4.7 Networks of theta neurons	12
5 Mean Field Reductions	13
5.1 The Ott-Antonsen manifold for fully connected networks	13
5.2 Dynamics of the mean field	13
5.3 The Ott-Antonsen extension to arbitrary network topologies	14
6 Investigation: Mean Field Reductions for undirected graphs	15
6.1 Directed graphs as permutations	15
6.2 Building the adjacency matrix	15
6.3 Results	15
7 Hebbian Learning	16
7.1 Fire and Wire	16
7.2 Anti-hebbian learning	16
8 Plasticity	17
8.1 Intrinsic plasticity	17
8.2 Spike-timing dependant plasticity	17
9 Investigation: Emerging Network Topologies	18
9.1 Redefinition of the network	18
9.2 Results	18
9.3 Discussion	18
10 Conclusion and discussion	19
11 References	20

A Appendix	22
A.1 Transformation to the QIF model	22
A.2 Solutions to the QIF model	22
A.2.1 Solving for $I < 0$	22
A.2.2 Solving for $I = 0$	22
A.2.3 Solving for $I > 0$	23
A.3 Frequency response of the neuron models	23
A.4 Jacobian of the Ott-Antonsen manifold	23
A.5 Jacobian of the Ott-Antonsen extended manifold	23

Abstract

Quisque nisl eros, pulvinar facilisis justo mollis, auctor consequat urna. Morbi a bibendum metus. Donec scelerisque sollicitudin enim eu venenatis. Duis tincidunt laoreet ex, in pretium orci vestibulum eget.

Acknowledgements

1 Nomenclature

i, e (or \exp)	Imaginary unit. Euler's number.
$n, \deg(n)$	Network node. Degree of node n .
N	Network degree. The number of neurons in the network.
A_{ij}	Adjacency matrix. Models which neuron i is connected to neuron j and vice-versa.
$\langle k \rangle$	Average node degree in the network.
\mathbf{k}	Node degree. Vector of the in- and out-degree of a single node as $(k^{\text{in}}, k^{\text{out}})$.
$\mathbf{k}^{\text{in}}, \mathbf{k}^{\text{out}}$	Node degree vector of all in- and out degrees of the network.
M_k	Number of unique node degrees in the network.
$P(k), P(\mathbf{k})$	Univariate and bivariate network degree distribution.
k_{\min}, k_{\max}	Smallest and largest degree found in a network.
γ	Degree exponent of a scale-free network.
p	Probability threshold of forming a link in random networks.
c	Assortativity of the network.
$\theta(t)_i$	Phase variable function of the theta model (of neuron i).
$\mathcal{P}_n(\theta)$	Pulse shaped synaptic coupling function.
κ	Macroscopic coupling strength.
$\eta_i, I(t)_i$	Excitability threshold and input current (of neuron i).
$g(\eta \eta_0, \sigma)$	Excitability threshold distribution with mean η_0 and width σ .
$Z(t)$	Kuramoto order parameter function.
$z(\mathbf{k}, t)$	Order parameter function for nodes with degree \mathbf{k} .
$\bar{Z}(t)$	Mean field order parameter function for arbitrary networks.
$S^{\text{in}}(t)_i, S^{\text{out}}(t)_i$	Spike trains received and emitted by neuron i as a sum of delta functions in time.
K_{ij}	Synaptic connectivity matrix. Strength of the connections between neurons i and j .
Δt_{ij}	Time difference between spikes of neurons i and j .
$W(\Delta t_{ij})$	Learning window. Models the correlation between synaptic strength and spike times.
$\phi(\Delta t_{ij})$	IP learning function. Models correlation between excitability strength and spike times.
\mathbb{T}	Set of angles in $[-\pi, \pi[$.
\mathbb{K}	Set of unique degrees in a network, support of P .
\mathbb{R}, \mathbb{C}	Set of real numbers. Set of complex numbers.
$F(v), F^{-1}(v)$	Random permutation and inverse permutation of the elements of a vector v .

2 Introduction

In 2013, one of the largest scientific projects ever funded by the European Union was launched. With the Human Brain Project [1], scientists and researchers aimed to reconstruct the human brain through supercomputer-based models and to advance neuroscience, medicine, and computing. Across the globe different fields of science are drawing inspiration from the human brain, through different approaches.

One such approach is to model the behaviour of biological neurons and to quantify the information processes in the brain from stimuli from the senses or from electrical and chemical processes in the body. A given neuron receives hundreds of impulses in the form of neurotransmitters, almost exclusively on its dendrites and cell body. These stimuli add up to an excitatory or inhibitory influence on the membrane potential of the neuron, so that the potential spikes when excitation is higher than an internal threshold. At this point, the neuron releases its own neurotransmitter and joins the interneuronal communication [2]. The neuron dynamics are largely captured by this spiking behaviour, on which most efforts have been concentrated. In 1952, Hodgkin and Huxley described a mathematical model for the action potentials in neurons, using a set of nonlinear differential equations that approximates the electrical characteristics of the neuron elements. In 1963 the authors were awarded the Nobel Prize in Physiology or Medicine [3] for their work.

As the human brain contains more than 100 billion neurons [4] it is unfeasible to study complex models at this scale. The topology of neuronal networks displays traits of small-worldness, wiring optimisation, and heterogeneous degree distributions [5], for which it is difficult to pin down one type of network architecture. Through the mean-field reduction (*MFR*) proposed in [6] one can reduce a large network of indistinguishable neurons to a low-dimensional dynamical system, described by the attraction of a mean-field variable to a reduced manifold. In this paper we will study the *MFR* of different types of networks of coupled theta neurons using the generalisations found in [7].

We distinguish between two types of dynamics: we study the dynamics of pulse-coupled networks *on* networks, and the dynamics *of* such networks is how they evolve over time. The dynamics of the network occur on a different (slower) time-scale than the dynamics on the network. Both types of dynamics influence each other [8].

3 Network Topologies

Networks consists of *nodes* n_j , $j \leq N$ connected by *links*. They arise in any context where objects are *related* to each other.

3.1 Representations and properties

We represent a finite network through the adjacency matrix: $A_{ij} = 1$ if there exists a relation from node j to node i and 0 otherwise. This means that A_{ij} can be *undirected* (symmetric) or *undirected*. If we think of the relations between guests at a party, then the social network is directed, as people might not know each other mutually. However, the network of people having shaken hands is symmetric. Self-links are an edge-case that depends on the context, as one generally does not shake hands with himself.

From A_{ij} we can compute the in- and out-degree vectors, which show how many links a node has coming in and out:

$$\mathbf{k}_i^{\text{in}} = \sum_{j=1}^N A_{ij} \quad \mathbf{k}_j^{\text{out}} = \sum_{i=1}^N A_{ij} \quad \deg(n_j) = \mathbf{k}_j = (\mathbf{k}_j^{\text{in}}, \mathbf{k}_j^{\text{out}}) \in \mathbb{K} \subset \mathbb{N} \quad (1)$$

The distribution of \mathbf{k}^{in} and \mathbf{k}^{out} is the most defining property of the network:

$$(\mathbf{k}^{\text{in}}, \mathbf{k}^{\text{out}}) \sim P(\deg(n) = \mathbf{k}) \quad (2)$$

The support of P is the set of unique degrees \mathbb{K} with cardinality M_k , which consists of integers. For symmetric networks, $\mathbf{k}^{\text{in}} = \mathbf{k}^{\text{out}}$, so that P is really a univariate distribution.

The average degree of the network is then:

$$\langle k \rangle = \frac{1}{N} \sum_{i,j=1}^{N,N} A_{ij} = \sum_{i=1}^N \mathbf{k}_i^{\text{in}} = \sum_{j=1}^N \mathbf{k}_j^{\text{out}} \quad (3)$$

3.2 Fixed-degree networks

A network consists of nodes, connected by links. The most simple network is one where all the nodes are connected, and so all nodes have a degree of N . In general, we can make networks where all nodes have the same degree, $\langle k \rangle$:

$$P(k) = \begin{cases} \langle k \rangle & \text{if } k = \langle k \rangle \\ 0 & \text{otherwise} \end{cases} \quad \mathbb{K} = \{\langle k \rangle\} \quad (4)$$

We will refer to these networks as fixed-degree networks.

3.3 Random / Erdös-Rényi networks

In 1959 Erdös and Rényi published their work on random graphs [9], where links are established if a random uniformly distributed number is higher than a threshold p . The degrees follow a binomial distribution:

$$P(k) = \binom{N-1}{k} p^k (1-p)^{N-1-k} \quad \mathbb{K} = [0, N] \quad (5)$$

with a mean $\mu = p(N - 1)$ and standard deviation $\sigma = \sqrt{\mu(1 - p)}$. For networks where $\langle k \rangle \ll N$, the network can be well approximated by a Poisson distribution:

$$P(k) = e^{-\langle k \rangle} \frac{\langle k \rangle^k}{k!} \quad \mathbb{K} = [0, N] \quad (6)$$

with a mean $\mu = \langle k \rangle$ and standard deviation $\sigma = \sqrt{\langle k \rangle}$. Both (5) and (6) describe similar quantities, but the latter is used more often due to its analytical simplicity [10].

3.4 Scale-free networks

What we can often observe in nature is the preferential attachment to nodes with a high degree [5]: the rich or famous tend to get more rich or famous. This trait is also described as the 80/20 rule by Pareto. Networks with this property consist of a small number of highly connected nodes, and a large number of low degree nodes. We can represent this with a power law distribution:

$$P(k) = Ak^{-\gamma} \quad \mathbb{K} = [k_{\min}, k_{\max}] \quad (7)$$

with A is a constant so that $\sum_{k=1}^{\infty} P(k) = 1$. We can also see that $A \sum_{k=1}^{\infty} k^{-\gamma} = 1$ so that $A = \sum_{k=1}^{\infty} k^{-\gamma} = 1/\zeta(\gamma)$, the Riemann Zéta function [10].

Networks with a distribution like (7) are called *scale-free* networks, as they lack an internal scale to represent the magnitude of the network: we can observe (7) on different scales like the probability of two Hollywood actors appearing in a movie, or the connections between web pages on the internet [11]. One description that comes close is the *natural cutoff* k_{\max} , the expected degree of the largest degree in the network. As we only expect the largest hub to be the only hub in the domain $[k_{\max}, +\infty]$:

$$\int_{k_{\max}}^{\infty} P(k) dk = \frac{1}{N}$$

For (7) this results in:

$$k_{\max} = k_{\min} \cdot N^{\frac{1}{\gamma-1}} \quad (8)$$

which shows that there might be large differences in size between the nodes.

There are constraints on γ to yield a scale-free network. When $0 < \gamma < 2$ the largest hub grows faster than N , so once its degree exceeds $N - 1$ there are no more new nodes to connect to and the network will not be able to grow according to (7). A rigorous proof is given in [12]. For $\gamma = 2$, the system grows linearly, as we can see in (8). When $2 < \gamma \leq 3$ we find the most scale-free networks, as for $\gamma > 3$ hubs are not sufficiently large and numerous to have much influence on the network [10].

4 The Theta Neuron Model

4.1 Modelling neuronal behaviour

Neurons communicate through *synapses* with electrical and chemical signals, in the form of action potentials and neurotransmitters respectively. We will speak of the presynaptic neuron as the neuron that sends a signal and of the postsynaptic neuron as the neuron that receives a signal. When the membrane voltage of a presynaptic neuron reaches an internal threshold, the neuron spikes (or fires) and an electrical signal travels down the neuron axons [2]. At the synapse, the electrical signal is converted into a chemical signal in the form of a neurotransmitter release of the presynaptic neuron, upon which the postsynaptic neuron receives the neurotransmitters and constructs its own electrical signal [13]. Most neurons in the central nervous system use either the excitatory neurotransmitter glutamate (AMPA or NMDA) or the inhibitory neurotransmitter GABA [14, 15].

As signals are converted from electrical to chemical and back, we will model the communication process as entirely electrical, consisting solely of action potentials. These will be modeled by a pulse-shaped curve, modulated by a dynamic variable of the neuron (for example the phase angle for the Theta neuron). The magnitude of the response of the postsynaptic neuron can be modeled by a coupling strength. The inhibitory/excitatory behavior can be modeled by allowing a negative/positive coupling strength between neurons [7, 16–18]. Another electrical communication process occurs when current flows between neurons proportional to the difference in their membrane voltages. We will avoid modeling the two communication modes at the same time, due to tractability [17].

4.2 Canonical neuron models

A number of neuron model families have been identified, and often there exists a continuous change of variables from models of the same family into a *canonical* model that can represent the whole family [19]. As the transformation is not required to be invertible, we can study the universal neurocomputational properties of the family in a low dimensional model. It was Hodgkin [20] who classified neurons into two types based on their excitability, upon experimenting with the electrical stimulation of cells. Class 1 models begin to spike at an arbitrarily slow rate, and the spiking frequency increases when the applied current is increased. Class 2 models spike as soon as their internal threshold is exceeded and the spiking frequency stays relatively constant within a certain frequency band [19].

4.3 Theta Neuron model description

In [21], a Class 1 canonical phase model was proposed:

$$\dot{\theta} = (1 - \cos \theta) + (1 + \cos \theta) \cdot I \quad \theta \in \mathbb{T} \quad (9)$$

with I a bifurcation parameter on the supplied current. We can visualise the dynamics on the unit circle, like in Figure 1. The neuron produces a spike when θ surpasses π , upon which $\theta \leftarrow -\pi$.

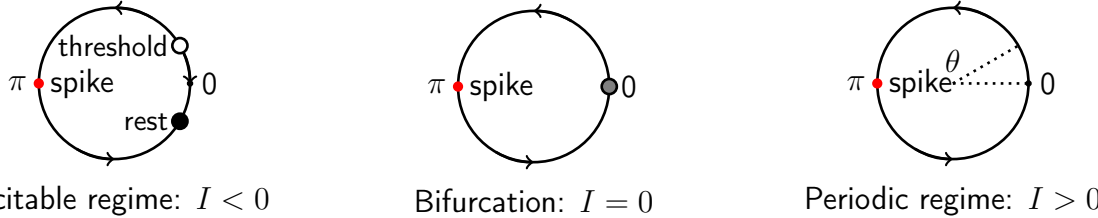


Figure 1: SNIC bifurcation of the theta neuron model. A spike occurs when $\theta = \pi$. For $I < 0$, the neuron is in a rest state but *excitable*. For $I > 0$, $\dot{\theta} > 0$ so that θ moves continuously around the circle and we can observe *periodic* sustained spiking. The saddle-node bifurcation occurs at $I = 0$, so that θ will spike when it is larger than 0.

We can recognise the features of the class 1 model in Figure 2. This makes (9) the normal form of the *saddle-node-on-invariant-circle (SNIC)* bifurcation [16].

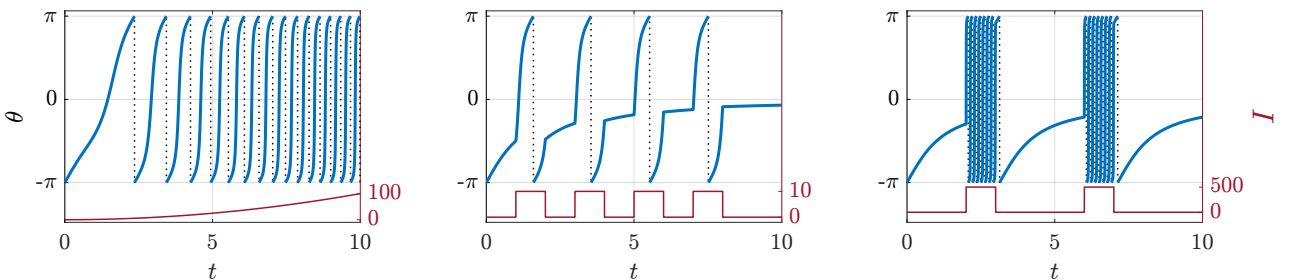


Figure 2: Properties of the theta neuron model, with solutions of (9) in blue, spikes marked in dotted lines, and the current I in red. Left: the spike frequency of θ increases as I is increased over time, which is the distinguishing feature of class 1 canonical models. Middle: spikes occur within a finite time period when $I > 0$ and within infinite time when $I = 0$. Right: when I is large, the neuron *bursts*.

Equilibria only exist for the *excitable* regime $I < 0$:

$$\begin{aligned}\dot{\theta} &= 1 - \cos \theta + I + I \cdot \cos \theta = (I + 1) + (I - 1) \cdot \cos \theta \\ \theta_{1,2}^* &= \pm \arccos\left(\frac{I+1}{1-I}\right) + 2\pi n\end{aligned}$$

We can find the stability of the equilibria through:

$$\frac{d}{d\theta}((1 - \cos \theta) + (1 + \cos \theta) \cdot I) = \sin \theta - \sin \theta \cdot I = (1 - I) \cdot \sin \theta$$

In the equilibria this yields:

$$\frac{d}{d\theta}(\theta_{1,2}^*) = \pm(1 - I) \cdot \sqrt{1 - \frac{I+1}{1-I}} = \pm(1 - I) \cdot \frac{2\sqrt{-I}}{1-I} = \pm 2\sqrt{-I}$$

This yields a stable equilibrium point for θ_1^* and an unstable for θ_2^* . This means that as θ gets perturbed above θ_2^* , a spike occurs and θ converges to θ_1^* . This is demonstrated in Figure 3.

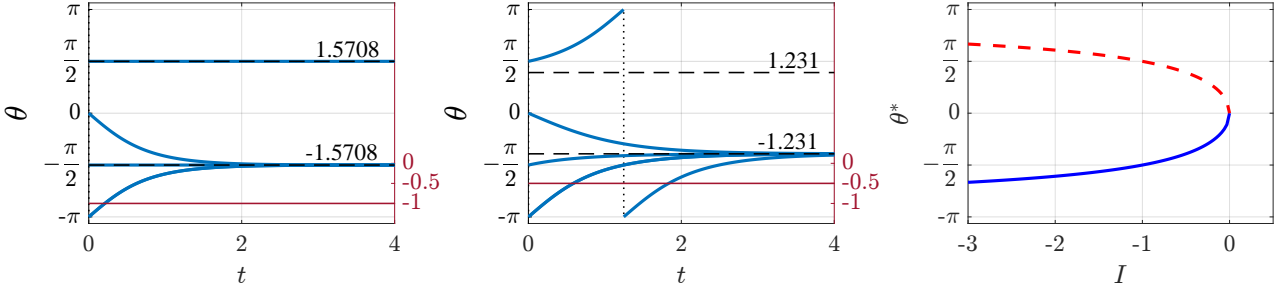


Figure 3: Equilibria θ^* for different values of I . Left: $I = -1$ yields $\theta_{1,2}^* = \pm \frac{\pi}{2}$, one of the simulations is started exactly on the unstable equilibrium. Middle: $I = -0.5$. Right: bifurcation diagram of the *SNIC* bifurcation, with the stable equilibria in blue, and the unstable in red.

4.4 Solutions for static currents

Gaining insight into (9) is hard, due to the difficulty of finding an analytical solution. However, it has been noted that there exists a simple transformation which yields (see A.1):

$$V \equiv \tan\left(\frac{\theta}{2}\right) \quad (10)$$

$$\dot{V} = V^2 + I \quad (11)$$

This model is called the *Quadratic Integrate and Fire model* (*QIF*). (11) models the membrane potential of a neuron, which spikes to $= \infty$ when the neuron spikes and is reset at $-\infty$. The transformation (10) is continuous between spikes, so insights from a solution for V can be transformed directly. The equilibria of the *QIF* model are simply $\pm\sqrt{I}$ so that we can express $\theta_{1,2}^* = 2 \cdot \arctan(\mp\sqrt{I})$, from [22].

The solution for the excitable regime $I < 0$ is :

$$V(t) = \frac{2\sqrt{-I}}{1 - e^{2t\sqrt{-I}}} - \sqrt{-I} \quad (12)$$

The solution at the bifurcation $I = 0$ is :

$$V(t) = \frac{-1}{t} \quad (13)$$

The solution for the periodic regime $I > 0$ is :

$$V(t) = -\sqrt{I} \cdot \cot(t\sqrt{I}) \quad (14)$$

These equations assume that at $t = 0$ a spike has occurred. The steps required to find (12)-(14) are described in A.2. Solutions for θ are found by taking the inverse of the transformation (10).

4.5 Frequency response

As we already saw in Figure 2, an increasing current increases the spiking frequency. We can compute this relationship by measuring how long it takes for V to reach a spike: we solve (14) for t at $V(t) = +\infty$ in A.3. This yields the oscillation period $T = \frac{\pi}{\sqrt{I}}$ which we can see in Figure 4. We know that when $\theta > \theta_2^*$ a spike occurs in the excitable regime, or in any case in the periodic regime. But the time that it takes to reach the spike can be arbitrarily long, depending on how far we are over θ_2^* . So, spikes will occur, but after a delay that is dependant on the stimulus. Explicitly, if we perturb $\theta(0) = \theta_2^* + \epsilon$ we obtain from [22]:

$$T_{\text{spike}} = \frac{-\tanh^{-1}\left(1 + \frac{\epsilon}{\sqrt{I}}\right)}{\sqrt{I}}$$

The delay to the spike blows up as $\varepsilon \rightarrow 0$ so that spikes may occur after a very large delay. In most of our future work, I will not be a static current. We ask ourselves: how sensitively does T depend on I when I is perturbed? We can measure this as a *relative* perturbation using dI/I and dT/T [2] :

$$\left| \frac{dT}{dI} \frac{I}{T} \right| = \left| \frac{dT/T}{dI/I} \right| = \left| -\frac{\pi}{2} \left(\frac{1}{\sqrt{I}} \right)^3 \frac{I}{T} \right| = \left| \frac{\pi}{2} \left(\frac{T}{\pi} \right)^3 \frac{I}{T} \right| = \frac{1}{2} \left| \left(\frac{T}{\pi} \right)^2 \cdot \left(\frac{\pi}{T} \right)^2 \right| = \frac{1}{2}$$

Hence, a 1% change in I will result in a 0.5 % change in the period.

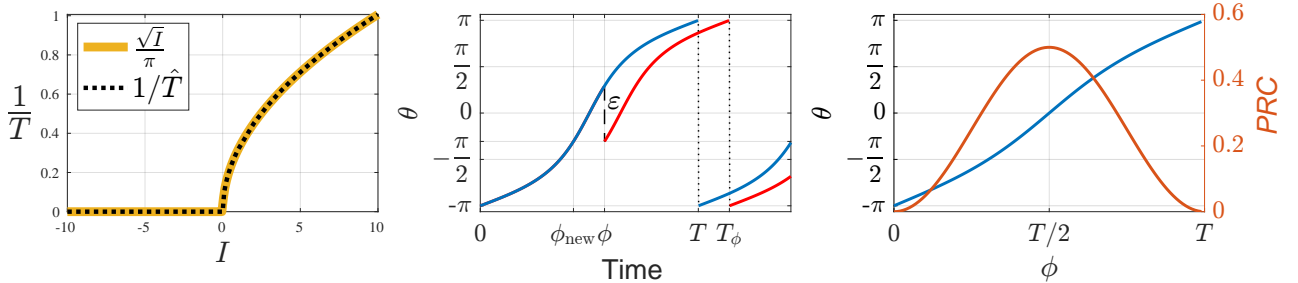


Figure 4: Response of the theta model to bifurcations on the frequency and the phase. Left: Frequency response of the theta model. For $I \leq 0$ the spike period is infinite, which is why we see the solutions to (9) approach $\theta = 0$ for $I = 0$. Middle: a bifurcation ε at time ϕ perturbs $\theta(t)$ (in blue) which results in a delayed spike (trajectory in red). Right: The PRC, (16) in red, with a solution for θ (in blue), to show when the model is the most susceptible to bifurcations.

4.6 Phase response

Perturbations on the period can also be understood from the perspective of the phase. Changes to the phase θ can delay or advance the event of a spike, and in general this depends on exactly when the stimulus occurs. The phase response curve (*PRC*) gives us exactly that relation [22, 23]. Let us define $\phi \in [0, T[$, which represents the time since the last event of a spike. When we add a small bifurcation $\varepsilon < 0$ to θ at time ϕ , a spike will occur at T_ϕ , and we have that $\theta(\phi_{\text{new}}) = \theta(\phi) + \varepsilon$. The time to the new spike is $T_\phi = T + (\phi - \phi_{\text{new}})$. The *PRC* can then be defined as:

$$PRC(\phi) = T_\phi - T \quad (15)$$

This process has been visualised in Figure 4, after [23]. For infinitesimally small perturbations to the phase, we can find the *PRC* as the *adjoint* of the solution, [22], as:

$$PRC(\phi) = \frac{1}{dV(\phi)/d\phi} = \frac{1}{2\sqrt{I}} \left(1 - \cos \left(\frac{2\pi}{T} \phi \right) \right) \quad (16)$$

We can use $\phi \in [0, T[$ and $\theta \in \mathbb{T}$ to see that (16) can be expressed as:

$$PRC(\theta) = \frac{1}{2\sqrt{I}} (1 + \cos \theta) \quad (17)$$

which is the magnitude with which I excites the model (9), [24]. Analysis of the *PRC* thus allows us to study how the bifurcation of θ with magnitude I occurs.

The *PRC* is always positive, which indicates that a positive bifurcation will advance the time of the spike, and vice versa. This has also been reported as a distinguishing feature of Class 1 models, [24].

4.7 Networks of theta neurons

We can easily extend the model to networks of neurons:

$$\dot{\theta}_i = (1 - \cos \theta_i) + (1 + \cos \theta_i) \cdot [\eta_i + I_i(t)] \quad \theta_i \in \mathbb{T}^N \quad (18)$$

$$I_i(t) = \frac{\kappa}{\langle k \rangle} \sum_{j=1}^N A_{ij} \cdot \mathcal{P}_n(\theta_j) \quad (19)$$

where the excitability η_i allows neuron i to adjust in which regime it is situated, and $\eta_i \sim g(\eta|\eta_0, \sigma)$. κ is the *synaptic* or *coupling* strength, and $\mathcal{P}_n(\theta) = a_n(1 - \cos \theta)^n$ models synaptic coupling by a pulse-shaped signal, emitted when a neuron fires. n models the sharpness of the pulse, and a_n is a normalisation constant so that $\int_0^{2\pi} \mathcal{P}_n d\theta = 2\pi$. We will take $n = 2$ from here, as in [7, 16, 17]. In (18) we see everything come together: changes to the phase θ_i are induced by $\dot{\theta}_i$ which in turn depends on the bifurcation of θ with magnitude I_i which depends on all neurons in the network.

Studying a set of differential equations like (19) is not feasible, as we are quickly approaching thousands of neurons. And in the end, the dynamics of a single neuron are not of interest. Instead, we wish to capture and study how the network behaves as a whole. One aspect, synchrony, can be captured by the Kuramoto order parameter:

$$Z(t) = \frac{1}{N} \sum_{j=1}^N e^{i\theta_j} \quad Z(t) \in \mathbb{C} \quad (20)$$

Z is a complex variable, consisting of a radius $r = |Z|$ and argument $\psi \arg(Z)$, so that $Z(t) = r(t)e^{i\psi(t)}$. When all phases are uniformly distributed across the unit circle \mathbb{T} , then $|Z| = 0$, resulting in a network with no synchronisation. When all phases are exactly the same, $|Z| = 1$, and the network is fully synchronised. (20) describes the *mean-field* of the network, a simpler model that describes the average behaviour of the whole network.

Different works on the dynamics of (20) have been published [16, 17], and we will build on that analysis in the following chapters.

5 Mean Field Reductions

5.1 The Ott-Antonsen manifold for fully connected networks

In [6, 25, 26] a method was published to predict the dynamics of the order parameter (20) for a fully connected network ($A_{ij} = 1$). The authors explore a continuum interpretation of the mean field, in the limit that $N \gg 1$. Using the fact that $\eta_i \sim g(\eta|\eta_0, \sigma)$, the number of neurons is constant, so that g is constrained by a continuity equation, and it is shown that there exists a manifold of invariant probability densities to which the dynamics are attracted to. We are left with a simplified description of the dynamics of the network, the *mean-field reduction* (*MFR*). The exact *MFR* is obtained by expanding g as a Fourier series, and expanding the pulse \mathcal{P}_n using the binomial theorem. When assuming η_i is distributed according to a Lorenz distribution:

$$g(\eta|\eta_0, \sigma) = \frac{1}{\pi} \frac{\sigma}{(\eta - \eta_0)^2 + \sigma^2} \quad (21)$$

the set of reduced equations then takes a particularly simple form, as the continuity equation can be evaluated at the poles of g using the Cauchy residue theorem for the integration of complex variables and one finds a closed form expression.

5.2 Dynamics of the mean field

Using this approach, the *MFR* becomes:

$$\dot{Z}(t) = -i \frac{(Z - 1)^2}{2} + \frac{(Z + 1)^2}{2} \cdot \left(-\sigma + i\eta_0 + ik \cdot \left(1 + \frac{Z^2 + \bar{Z}^2}{6} - \frac{4}{3}\text{Re}(Z) \right) \right) \quad (22)$$

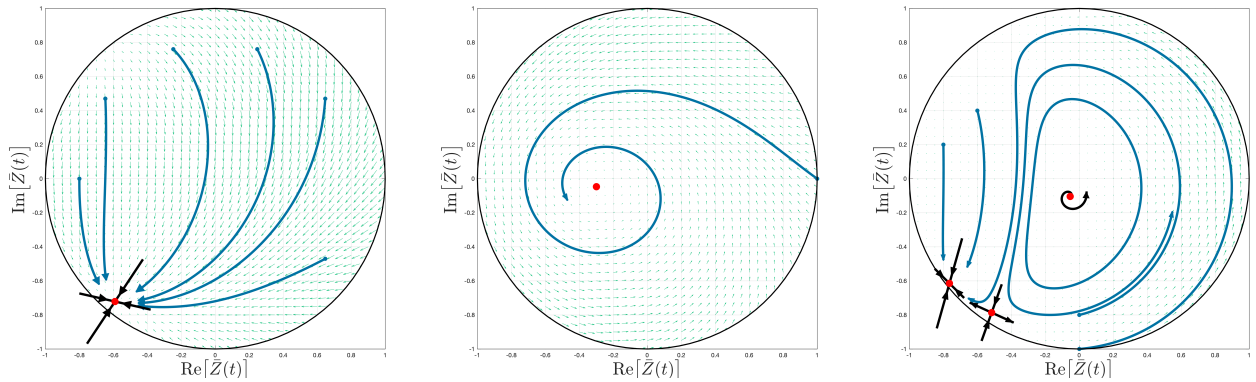
We can now describe the mean-field dynamics using (22), and as it is a complex-valued function, the reduced system is two-dimensional, with three bifurcation parameters η_0, σ and k . For a fully connected network, three distinct macroscopic states can be identified.

In the partially synchronous rest state (*PSR*) we can observe in Figure 5a, $\bar{Z}(t)$ settles onto a stable node. Most neurons can be found in a resting state $\eta_0 + \sigma \lesssim 0$, and inhibit one another through $k < 0$. Most neurons are therefore inactive, though some spiking neurons from the tail of $g(\eta)$ are present but have a negligible effect.

In Figure 5b we can observe a partially synchronous spiking (*PSS*) state, where we can see how $\bar{Z}(t)$ settles onto a stable focus. This happens predominantly when $\eta_0 - \sigma \gtrsim 0$ and most neurons inherently spike, with the coupling being either excitatory or weakly inhibitory. Although most neurons are active, the network is partially synchronous and organized such that phase cancellation occurs by continuous spiking among the neurons.

Lastly, in the collective periodic wave state (*CPW*) we can observe a limit cycle of the mean field, in Figure 5c. Most neurons are active and inhibitory: $\eta_0 > 0$ and $k < 0$. The collective oscillation emerges from the interplay between the neurons' inherent tendency to spike and the strong suppressive network interaction. *CPW* states are mediated through Hopf bifurcations and homoclinic bifurcations of $Z(t)$. We can also see the occurrence of a saddle-node bifurcation in the lower hand corner, for low σ . We will continue to study the *CPW* due to their interesting properties.

A more detailed discussion of the different regimes and bifurcations can be found in [16].



(a) PSR state for $\eta_0 = -0.9, \sigma = 0.8$ and $\kappa = -2$. The mean field settles onto a stable node.

(b) PSS state for $\eta_0 = 0.5, \sigma = 0.7$ and $\kappa = 2$. The mean field settles onto a stable focus.

(c) CPW state for $\eta_0 = 10.75, \sigma = 0.5$ and $\kappa = -9$. The mean field settles onto a stable limit cycle.

Figure 5: Three macroscopic states observed in the *MFR* inside the imaginary unit circle $|\bar{Z}(t)| = 1$. Green arrows mark the phase space vector field and blue trails mark solution curves. Red points indicate equilibrium points, with black arrows marking the direction of the eigenvectors in that point, scaled according to the magnitude of the corresponding eigenvalues.

5.3 The Ott-Antonsen extension to arbitrary network topologies

In [7] the authors extended their work to include networks with arbitrary degree distributions.

6 *Investigation: Mean Field Reductions for undirected graphs*

6.1 Directed graphs as permutations

Lorem ipsum dolor sit amet, consectetur adipiscing elit. Quisque nisl eros, pulvinar facilisis justo mollis, auctor consequat urna. Morbi a bibendum metus. Donec scelerisque sollicitudin enim eu venenatis. Duis tincidunt laoreet ex, in pretium orci vestibulum eget.

6.2 Building the adjacency matrix

We can find an exact solution for A given the degree vectors in (2). A_{ij} represents a directed graph, but $A_{ij} \neq A_{ji}$ is not a necessary condition. For the elements of A_{ij} we need to find N^2 number of variables. We have the following constraints:

1. The column- and row-sums of A_{ij} must be equal to \mathbf{k}^{in} and \mathbf{k}^{out} , see (1). $2N$ constraints.
2. Self-coupling is mandatory: $A_{ii} = 1$. N constraints.
3. The total number of links is constant: $\sum_{i=1}^N \mathbf{k}_i^{\text{in}} \equiv \sum_{j=1}^N \mathbf{k}_j^{\text{out}} \equiv \sum_{i,j=1}^N A_{ij}$. 1 constraint.

This means that there are $N^2 - (3N + 1)$ variables to find. Once a solution has been found, A_{ij} can be switched with element A_{ic} if $A_{ij} \neq A_{ic}$ and A_{rj} with A_{rc} , which yields a new feasible solution. The number of switches one can make is high, and therefore we can simply try a stochastic approach to obtain A :

1. Choose a random row $i \in [1, N]$. $A_{i,i} = 1$, so we need $m = \mathbf{k}_i^{\text{in}} - 1$ elements that are 1.
2. Perform $F(\mathbf{k}_j^{\text{out}}, j \neq i)$ and therein find the indices ℓ of the m first largest elements.
3. Set $A_{il} = 1 \forall l \in F^{-1}(\ell)$.

Algorithms that find the largest value in a vector start from the first or the last element. The permutation allows us to find different maxima every time by shuffling the vector.

6.3 Results

Lorem ipsum dolor sit amet, consectetur adipiscing elit. Quisque nisl eros, pulvinar facilisis justo mollis, auctor consequat urna. Morbi a bibendum metus. Donec scelerisque sollicitudin enim eu venenatis. Duis tincidunt laoreet ex, in pretium orci vestibulum eget.

7 Hebbian Learning

7.1 Fire and Wire

Lorem ipsum dolor sit amet, consectetur adipiscing elit. Quisque nisl eros, pulvinar facilisis justo mollis, auctor consequat urna. Morbi a bibendum metus. Donec scelerisque sollicitudin enim eu venenatis. Duis tincidunt laoreet ex, in pretium orci vestibulum eget.

7.2 Anti-hebbian learning

Lorem ipsum dolor sit amet, consectetur adipiscing elit. Quisque nisl eros, pulvinar facilisis justo mollis, auctor consequat urna. Morbi a bibendum metus. Donec scelerisque sollicitudin enim eu venenatis. Duis tincidunt laoreet ex, in pretium orci vestibulum eget.

8 Plasticity

8.1 Intrinsic plasticity

Lorem ipsum dolor sit amet, consectetur adipiscing elit. Quisque nisl eros, pulvinar facilisis justo mollis, auctor consequat urna. Morbi a bibendum metus. Donec scelerisque sollicitudin enim eu venenatis. Duis tincidunt laoreet ex, in pretium orci vestibulum eget.

8.2 Spike-timing dependant plasticity

Lorem ipsum dolor sit amet, consectetur adipiscing elit. Quisque nisl eros, pulvinar facilisis justo mollis, auctor consequat urna. Morbi a bibendum metus. Donec scelerisque sollicitudin enim eu venenatis. Duis tincidunt laoreet ex, in pretium orci vestibulum eget.

9 *Investigation: Emerging Network Topologies*

9.1 Redefinition of the network

Lorem ipsum dolor sit amet, consectetur adipiscing elit. Quisque nisl eros, pulvinar facilisis justo mollis, auctor consequat urna. Morbi a bibendum metus. Donec scelerisque sollicitudin enim eu venenatis. Duis tincidunt laoreet ex, in pretium orci vestibulum eget.

9.2 Results

Lorem ipsum dolor sit amet, consectetur adipiscing elit. Quisque nisl eros, pulvinar facilisis justo mollis, auctor consequat urna. Morbi a bibendum metus. Donec scelerisque sollicitudin enim eu venenatis. Duis tincidunt laoreet ex, in pretium orci vestibulum eget.

9.3 Discussion

Lorem ipsum dolor sit amet, consectetur adipiscing elit. Quisque nisl eros, pulvinar facilisis justo mollis, auctor consequat urna. Morbi a bibendum metus. Donec scelerisque sollicitudin enim eu venenatis. Duis tincidunt laoreet ex, in pretium orci vestibulum eget.

10 Conclusion and discussion

Test citations: In [17]

11 References

- [1] Human Brain Project., 2017. <https://www.humanbrainproject.eu/en/>. Accessed: 28.05.2020.
- [2] C. Börgers, *An Introduction to Modeling Neuronal Dynamics*. Texts in Applied Mathematics. Springer International Publishing, 2018.
- [3] The Nobel Prize in Physiology or Medicine 1963., 2009. <https://www.nobelprize.org/prizes/medicine/1963/speedread/>. Accessed: 28.05.2020.
- [4] S. Herculano-Houzel, *The Human Brain in Numbers: A Linearly Scaled-up Primate Brain*. *Frontiers in human neuroscience* **3** (11, 2009) 31.
- [5] E. Bullmore and D. Bassett, *Brain Graphs: Graphical Models of the Human Brain Connectome*. *Annual review of clinical psychology* **7** (04, 2010) 113–40.
- [6] E. Ott and T. M. Antonsen, *Low Dimensional Behavior of Large Systems of Globally Coupled Oscillators*. [arXiv:0806.0004 \[nlin.CD\]](https://arxiv.org/abs/0806.0004).
- [7] S. Chandra, D. Hathcock, K. Crain, T. Antonsen, M. Girvan, and E. Ott, *Modeling the Network Dynamics of Pulse-Coupled Neurons*. *Chaos (Woodbury, N.Y.)* **27** (03, 2017) 10.
- [8] T. Gross and H. Sayama, *Adaptive networks: theory, models and applications*. Springer International Publishing, January, 2009.
- [9] P. Erdos and A. Rényi, *On Random Graphs I*. *Publicationes Mathematicae* **6** (1959) 290–297.
- [10] A. Barabási, *Network Science*. Cambridge University Press, 2016. <https://books.google.dk/books?id=iLtGDQAAQBAJ>.
- [11] A.-L. Barabási and E. Bonabeau, *Scale-Free Networks*. *Scientific American* **288** no. 60-69, (2003) 50–59. <http://www.nd.edu/~networks/PDF/Scale-Free%20Sci%20Amer%20May03.pdf>.
- [12] C. I. Del Genio, T. Gross, and K. E. Bassler, *All Scale-Free Networks Are Sparse*. *Phys. Rev. Lett.* **107** (Oct, 2011) 178701. <https://link.aps.org/doi/10.1103/PhysRevLett.107.178701>.
- [13] The University Of Queensland Brain Institute, *Action potentials and synapses*. <https://qbi.uq.edu.au/brain-basics/brain/brain-physiology/action-potentials-and-synapses>. Composed: 09/11/2017. Accessed: 02/10/2020.
- [14] B. Ermentrout and D. Terman, *The Mathematical Foundations of Neuroscience*. vol. Vol. 35. Springer, July, 2010.
- [15] X. Zhang and J. Feng, *Computational modeling of neuronal networks*. [arXiv:1203.0868 \[q-bio.NC\]](https://arxiv.org/abs/1203.0868).
- [16] T. Luke, E. Barreto, and P. So, *Complete Classification of the Macroscopic Behavior of a Heterogeneous Network of Theta Neurons*. *Neural Computation* **25** (12, 2013) 1–28.

- [17] C. Bick, M. Goodfellow, C. Laing, and E. Martens, *Understanding the dynamics of biological and neural oscillator networks through exact mean-field reductions: a review*. *Journal of Mathematical Neuroscience* **10** no. 1, (Dec., 2020) .
- [18] E. Montbrió, D. Pazó, and A. Roxin, *Macroscopic Description for Networks of Spiking Neurons*. *Physical Review X* **5** no. 2, (Jun, 2015) 14. <http://dx.doi.org/10.1103/PhysRevX.5.021028>.
- [19] F. C. Hoppensteadt and E. M. Izhikevich, *Canonical Neural Models.*, 2001.
- [20] A. Hodgkin, *The local electric changes associated with repetitive action in a non-medullated axon*. *The Journal of physiology* **107** no. 2, (March, 1948) 165—181. <https://www.ncbi.nlm.nih.gov/pmc/articles/pmid/16991796/?tool=EBI>.
- [21] B. Ermentrout and N. Kopell, *Parabolic Bursting in an Excitable System Coupled with a Slow Oscillation*. *Siam Journal on Applied Mathematics - SIAMAM* **46** (04, 1986) 233–253.
- [22] B. Gutkin, *Theta-Neuron Model*. Springer New York, New York, NY, 2013. https://doi.org/10.1007/978-1-4614-7320-6_153-1.
- [23] F. A. Pérez, *Phase-responsiveness transmission in a network of quadratic integrate-and-fire neurons*. Universitat Politècnica de Catalunya, Facultat de Matemàtiques i Estadística (January, 2020) . Bachelor Thesis.
- [24] B. Ermentrout, *Type i Membranes, Phase Resetting Curves, and Synchrony* *Neural Comput.* **8** no. 5, (July, 1996) 979–1001. <https://doi.org/10.1162/neco.1996.8.5.979>.
- [25] E. Ott and T. M. Antonsen, *Long Time Evolution of Phase Oscillator Systems*. [arXiv:0902.2773 \[nlin.CD\]](https://arxiv.org/abs/0902.2773).
- [26] E. Ott, B. R. Hunt, and T. M. Antonsen, *Comment on "Long Time Evolution of Phase Oscillator Systems"* [*Chaos* 19, 023117 (2009), arXiv: 0902.2773]. [arXiv:1005.3319 \[nlin.CD\]](https://arxiv.org/abs/1005.3319).

A Appendix

A.1 Transformation to the QIF model

We prove that the transformation (10) holds from the QIF model (11) to the Theta model (9).

$$V \equiv \tan\left(\frac{\theta}{2}\right) \quad \longrightarrow \quad \frac{dV}{dt} = \frac{1}{2 \cos^2\left(\frac{\theta}{2}\right)} \frac{d\theta}{dt}$$

Insert into $\frac{dV}{dt} = V^2 + I$:

$$\frac{d\theta}{dt} = 2\left(\cos^2\left(\frac{\theta}{2}\right) \cdot \tan^2\left(\frac{\theta}{2}\right) + \cos^2\left(\frac{\theta}{2}\right) \cdot I\right) = 2\left(\sin^2\left(\frac{\theta}{2}\right) + \cos^2\left(\frac{\theta}{2}\right) \cdot I\right)$$

Using $\cos^2\left(\frac{\theta}{2}\right) = \frac{1+\cos(\frac{\theta}{2})}{2}$ and $\sin^2\left(\frac{\theta}{2}\right) = \frac{1-\cos(\frac{\theta}{2})}{2}$:

$$\dot{\theta} = 2\left(\frac{1-\cos\theta}{2} + \left(\frac{1+\cos\theta}{2}\right) \cdot I\right) = (1-\cos\theta) + (1+\cos\theta) \cdot I$$

This proves that the transformation (10) is correct.

A.2 Solutions to the QIF model

Depending on the value of I , we can distinguish multiple solutions [23]. In all cases we can integrate through the separation of variables. Solutions are bound to start at $V(t_0)$, right after a spike has occurred at $t = t_0$.

A.2.1 Solving for $I < 0$

$$\begin{aligned} \int_{V(t_0)}^{V(t)} \frac{dv}{v^2 - \tilde{I}^2} &= \int_{V(t_0)}^{V(t)} \frac{dv}{(v + \tilde{I})(v - \tilde{I})} = \frac{1}{2\tilde{I}} \int_{V(t_0)}^{V(t)} \frac{dv}{v - \tilde{I}} - \frac{1}{2\tilde{I}} \int_{V(t_0)}^{V(t)} \frac{dv}{v + \tilde{I}} \\ &= \frac{1}{2\tilde{I}} \log\left(1 - \frac{2\tilde{I}}{v + \tilde{I}}\right) \Big|_{V(t_0)}^{V(t)} = \int_{t_0}^t d\tau = t - t_0 \\ V(t) &= \lim_{V(t_0) \rightarrow -\infty} \frac{2\sqrt{-I}}{1 - \left(1 - \frac{2\sqrt{-I}}{V(t_0) + \sqrt{-I}}\right) \cdot e^{2(t-t_0)\sqrt{-I}}} - \sqrt{-I} \\ &= \frac{2\sqrt{-I}}{1 - e^{2(t-t_0)\sqrt{-I}}} - \sqrt{-I} \end{aligned}$$

A.2.2 Solving for $I = 0$

$$\begin{aligned} \int_{V(t_0)}^{V(t)} \frac{dv}{v^2} &= \frac{1}{v} \Big|_{V(t_0)}^{V(t)} = -\frac{1}{V(t)} + \frac{1}{V(t_0)} = \int_{t_0}^t d\tau = t - t_0 \\ V(t) &= \lim_{V(t_0) \rightarrow -\infty} \frac{V(t_0)}{1 - V(t_0)(t - t_0)} \stackrel{H}{=} \frac{-1}{t - t_0} \end{aligned}$$

A.2.3 Solving for $I > 0$

$$\begin{aligned}
\int_{V(t_0)}^{V(t)} \frac{dv}{v^2 + I} &= \int_{V(t_0)}^{V(t)} \frac{I}{\left(\frac{v}{\sqrt{I}}\right)^2 + 1} dv \stackrel{x=\frac{v}{\sqrt{I}}}{=} \int_{\frac{V(t_0)}{\sqrt{I}}}^{\frac{V(t)}{\sqrt{I}}} \frac{I}{x^2 + 1} dx = \frac{1}{\sqrt{I}} \arctan(x) \Big|_{\frac{V(t_0)}{\sqrt{I}}}^{\frac{V(t)}{\sqrt{I}}} \\
&= \frac{1}{\sqrt{I}} \left(\arctan\left(\frac{V(t)}{\sqrt{I}}\right) - \arctan\left(\frac{V(t_0)}{\sqrt{I}}\right) \right) = \int_{t_0}^t d\tau = t - t_0 \\
V(t) &= \lim_{V(t_0) \rightarrow -\infty} \sqrt{I} \cdot \tan\left((t - t_0)\sqrt{I} + \arctan\left(\frac{V(t_0)}{\sqrt{I}}\right)\right) = \sqrt{I} \cdot \tan\left((t - t_0)\sqrt{I} - \frac{\pi}{2}\right) \\
&= \sqrt{I} \cdot \cot\left((t - t_0)\sqrt{I}\right)
\end{aligned}$$

A.3 Frequency response of the neuron models

The integral is solved like before, but now with the conditions of the spike:

$$\begin{aligned}
T &= \lim_{a \rightarrow \infty} \int_{-a}^a \frac{I}{\left(\frac{v}{\sqrt{I}}\right)^2 + 1} dv \stackrel{x=\frac{v}{\sqrt{I}}}{=} \lim_{a \rightarrow \infty} \int_{-\frac{a}{\sqrt{I}}}^{\frac{a}{\sqrt{I}}} \frac{I}{x^2 + 1} dx = \lim_{a \rightarrow \infty} \frac{1}{\sqrt{I}} \arctan(x) \Big|_{-\frac{a}{\sqrt{I}}}^{\frac{a}{\sqrt{I}}} \\
&= \frac{1}{\sqrt{I}} \left(\frac{\pi}{2} - \left(-\frac{\pi}{2}\right) \right) = \frac{\pi}{\sqrt{I}}
\end{aligned}$$

So the frequency of oscillation is proportional to \sqrt{I} .

A.4 Jacobian of the Ott-Antonsen manifold

A.5 Jacobian of the Ott-Antonsen extended manifold